Local and Global Dynamics of Unentangled Polyethylene Melts by ^{13}C NMR

XiaoHua Qiu and M. D. Ediger*

Department of Chemistry, University of Wisconsin−Madison, Madison, Wisconsin 53706

Received July 7, 1999

ABSTRACT: ^{13}C NMR T_1, NOE, and $T_{1\rho}$ were measured for two unentangled polyethylene melts ($C_{44}H_{90}$ and $M_w = 2150$ g/mol) at 5, 25, and 75 MHz ^{13}C Larmor frequency from the melting points up to 260 °C. The data were fit with a model composed of a fast segmental relaxation and a long time tail described by Rouse modes. The fitting parameters are consistent with MD computer simulations on similar systems and independent experiments such as viscosity and self-diffusion coefficient measurements. Polyethylene is an unusual polymer in that it has a very pronounced long time tail in the C−H vector correlation function. This long time tail makes this experiment a sensitive tool with which to characterize the global dynamics of polyethylene melts. Rouse modes, with corrections suggested from MD simulation, were found to be an adequate description of the global dynamics in this molecular weight range. The activation energy for the conformational dynamics was found to be 4 kcal/mol, which is significantly less than the flow activation energy. Therefore, in contrast to some other well-studied examples, conformational transitions are not the fundamental motions for flow in polyethylene. MD computer simulations of $C_{44}H_{90}$ [Smith et al. *Macromolecules* **1995**, *28*, 5897] using an explicit atom model closely reproduce the experimental data.

I. Introduction

^{13}C NMR relaxation time measurements such as the spin−lattice relaxation time T_1 and the nuclear Overhauser effect NOE have long been used to characterize local dynamics in polymer melts.[1] The main relaxation mechanism for these measurements is typically dipolar relaxation caused by the reorientation of a C−H vector. Since conformational transitions result in significant C−H vector reorientation,[2] conventional analysis and interpretation of such experiments have been based on models[3−7] that describe the conformational dynamics in polymer melts. Such models have been successfully used to analyze and interpret T_1 and NOE data on various polymers.[7,8]

Despite the substantial C−H vector reorientation induced by conformational dynamics, a C−H vector on a polymer chain cannot completely forget its starting orientation until the whole chain has time to relax. In other words, the C−H vector orientation autocorrelation function (OACF) does not decay to zero until the longest relaxation time of the chain is reached. The time scale for the relaxation of the entire chain can be thousands of times longer than the time scale for conformational dynamics depending on the length of the chain. Therefore, the C−H vector OACF can be qualitatively characterized as two separate processes: very fast segmental motions which account for most of the decay and much slower chain motions forming a long time tail which persists until the longest relaxation time of the chain. Working with biopolymers which have restricted conformational dynamics, the bio-NMR community has utilized this bimodal distribution of relaxation times for the C−H vector OACF for some time. In fact, the two different relaxation time scales form the basis for the well-accepted "model-free" approach.[9]

As compared to a structured biopolymer, the weight of the long time tail is significantly smaller for synthetic polymers which have less restricted conformational dynamics. In fact, this long time tail was not invoked in earlier studies of synthetic polymers.[7,10,11] The long time tail is difficult to observe experimentally because the Larmor frequency used in NMR studies is usually high compared to the inverse of the relaxation times of the long time tail. One unsatisfactory result is that high-field T_1 and NOE measurements have been perceived as irrelevant in characterizing the global dynamics of synthetic polymers, a very important academic and industrial problem. Other experimental techniques and data analysis procedures have been developed to investigate this long time tail.[12−15]

Despite the above perception, our preliminary ^{13}C NMR T_1 and NOE study[16] on $C_{44}H_{90}$, a short polyethylene, showed that there is a long time tail noticeable in the data. MD simulations of $C_{44}H_{90}$[17] and $C_{100}H_{202}$[18] not only found a noticeable long time tail in the C−H vector OACF but also characterized the long time tail in terms of both weight and relaxation time. To understand the effect of the long time tail on NMR relaxation time measurements and to investigate the feasibility of using such measurements to study global polymer dynamics,^{13}C T_1, NOE, and $T_{1\rho}$ (spin−lattice relaxation time in the rotating frame) were measured in this study for two unentangled polyethylenes: $C_{44}H_{90}$ and a polyethylene with $M_w = 2150$ g/mol. Polyethylene was chosen also because its technical importance and structural simplicity have made it an extensively studied polymer melt system both by experiments[19−24] and simulations.[25−29] Those studies provided detailed information for the analysis and interpretation of our experimental data.

In this experiment, dynamical information at 2 kHz and in the range 5−375 MHz was probed. Coupled with a wide temperature range of 90−260 °C, our experiment covered the frequency window relevant for the long time tail relaxation in both polyethylene melts. The wide range in terms of both frequency and temperature provided a powerful tool to characterize the dynamics that contribute to C−H vector reorientation in the two systems. A model consisting of a fast segmental relaxation and a long time tail described by Rouse modes[30,31] was developed and found to be a good description of the

* To whom correspondence should be addressed.

10.1021/ma991086n CCC: $19.00
Published on Web 12/28/1999

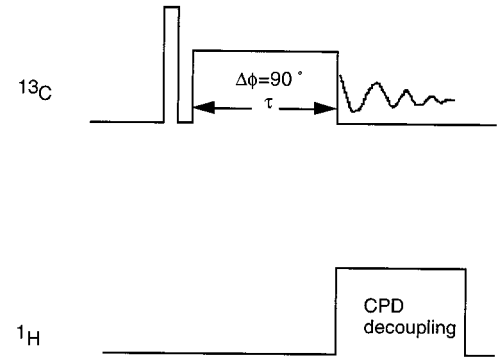

Figure 1. Pulse sequence for the observation of the ^{13}C rotating-frame spin−lattice relaxation time, $T_{1\rho}$. The locking field is 90° phase shifted with respect to the 90° pulse.

C−H vector OACF. The fitting parameters are consistent with MD simulations on similar systems and independent experiments such as viscosity and self-diffusion coefficient measurements. On the basis of the success of the model, a procedure was developed to predict ^{13}C T_1, NOE, and $T_{1\rho}$ of unentangled polyethylene melts of any molecular weight.

II. Experimental Section

Materials. Polyethylene with $M_w = 2150$ g/mol and polydispersity <1.15 (designated as PE2K in this paper) was purchased from Scientific Polymer. Normal tetratetracontane, $C_{44}H_{90}$, was purchased from Aldrich. All samples contained 1 g of material in a 10 mm Wilmad NMR tube. The samples were degassed under vacuum for 1 day at room temperature, then for another day above the melting temperature, and finally sealed under vacuum. The methylenes on the backbone of polyethylene showed up as a dominating peak at 30 ppm in the ^{13}C spectrum. Five carbons at the ends of the chains were resolved by chemical shift but are not discussed in this paper.

NMR Measurements. All measurements were performed at 75.47, 25.26, and 5.06 MHz ^{13}C Larmor frequency on a Bruker DMX-300 spectrometer specially designed for frequent field change. A homemade probe utilizing solenoid geometry and optimized for high-temperature experiments[32] was used for all measurements from the melting temperature of the sample (90 °C for $C_{44}H_{90}$ and 130 °C for PE2K) to 260 °C. Temperature was calibrated by observing the sudden spectrum change as the melting point of chosen compounds (T_m from 60 to 260 °C) was crossed. The calibration was performed twice after each magnetic field change, and very little deviation was noticed. This calibration method yielded a temperature accuracy of ±1 K. The Bruker temperature controller was able to control the temperature to within ±0.1 K during the experiment.

T_1 was measured by a $\pi-t-\pi/2$ pulse sequence, waiting at least $8T_1$ between scans. NOE was measured by the comparison of spectrum with continuous decoupling and the one with inverse-gated decoupling, waiting at least $10T_1$ between scans. Details of the measurements have been described previously.[33] One, eight, and 2000 scans were collected for signal averaging for 75, 25, and 5 MHz, respectively. T_1 values are believed to be accurate within 2% and NOEs within ±0.02, except for 5 MHz, where NOEs are accurate within ±0.15.

The $T_{1\rho}$ measurements followed the description by Ohuchi et al.,[34] and the pulse sequence is shown in Figure 1. The 90° pulse was around 18 μs. Since the delay time τ might be long for the experiment, only very weak locking power was employed to avoid heating the sample. The actual power used was equivalent to the magnetic field for 2 kHz ^{13}C Larmor frequency. Following the delay time, the spectrum was collected. An exponential fit to the data yielded the time constant $T_{1\rho}$. The decoupling field was turned on only during the FID collection time to avoid any complications from the decoupling source during the locking time.[34] The center of the spectrum was carefully set to be less than 5 Hz away from the main peak to avoid any errors caused by off-resonance conditions. All $T_{1\rho}$ data were collected at 75.47 MHz ^{13}C Larmor frequency.

Relaxation Equations. For aliphatic carbons, previous study[35] as well as the NOE data of $C_{44}H_{90}$ (NOE very close to 3 at high temperature) indicates that the only significant relaxation mechanism is dipolar coupling to directly bonded protons. The C−H bond vector second-order autocorrelation function (OACF) is given by

$$G(t) = {}^1/_2\langle 3\cos^2\theta(t) - 1\rangle \quad (1)$$

where $\theta(t)$ describes the orientation of a C−H bond vector at time t relative to its orientation at time $t = 0$. The brackets $\langle\ \rangle$ indicate an average over equivalent C−H bond vectors and over all possible arbitrary starting times $t = 0$. The spectral density function $J(\omega)$ is the Fourier transform of $G(t)$:

$$J(\omega) = {}^1/_2\int_{-\infty}^{+\infty} G(t)e^{i\omega t}\,dt \quad (2)$$

T_1, NOE, and $T_{1\rho}$ can be expressed in terms of $J(\omega)$:

$$\frac{1}{T_1} = Kn[J(\omega_H - \omega_C) + 3J(\omega_C) + 6J(\omega_H + \omega_C)] \quad (3)$$

$$\mathrm{NOE} = 1 + \frac{\gamma_H}{\gamma_C}\left[\frac{6J(\omega_H + \omega_C) - J(\omega_H - \omega_C)}{J(\omega_H - \omega_C) + 3J(\omega_C) + 6J(\omega_H + \omega_C)}\right] \quad (4)$$

$$\frac{1}{T_{1\rho}} = {}^1/_2Kn[4J(\omega_e) + J(\omega_H - \omega_C) + 3J(\omega_C) + 6J(\omega_H) + 6J(\omega_H + \omega_C)] \quad (5)$$

where ω_H and ω_C are the resonance frequencies of ^1H and ^{13}C, ω_e is the spin-locking field, n is the number of bonded protons, and K is a constant whose value is calculated to be 2.29×10^9 s^{-2}.[16] γ_H and γ_C are the gyromagnetic ratios for ^1H and ^{13}C.

III. Results

Figure 2 shows T_1 and NOE data of PE2K at 5, 25, and 75 MHz ^{13}C Larmor frequency. Various lines in the figure are fits and predictions of a model that will be explained in the Discussion section. Figure 3 shows T_1 and NOE data of $C_{44}H_{90}$ at 25 and 75 MHz ^{13}C Larmor frequency. Figure 4 shows $T_{1\rho}$ data of both samples at 75 MHz ^{13}C Larmor frequency main field and 2 kHz locking field. In both Figure 3 and Figure 4, predictions from the model are shown as dashed lines.

IV. Discussion

A. The Model. Figure 5 shows a sketch of C−H vector reorientation in polyethylene mapped onto a bead−spring model. The decay of the C−H vector orientation autocorrelation function occurs primarily by conformational transitions which take place on a very short time scale. However, on that short time scale, the vector connecting two beads (the spring vector) cannot reorient significantly, so a C−H vector does not uniformly explore all possible orientations but rather has some tendency to be perpendicular to the spring vector. The randomization of the orientation of a C−H vector cannot be complete until the spring vector has reoriented significantly, which occurs on a time scale much longer than the one for conformational dynamics. It is natural to use the Rouse model to describe the reorientation of the spring vector.

Such a long time tail is evident in MD simulations[18,36] of unentangled polyethylene melts. It is also indicated by the fact that NOE < 3 at 75 MHz ^{13}C Larmor

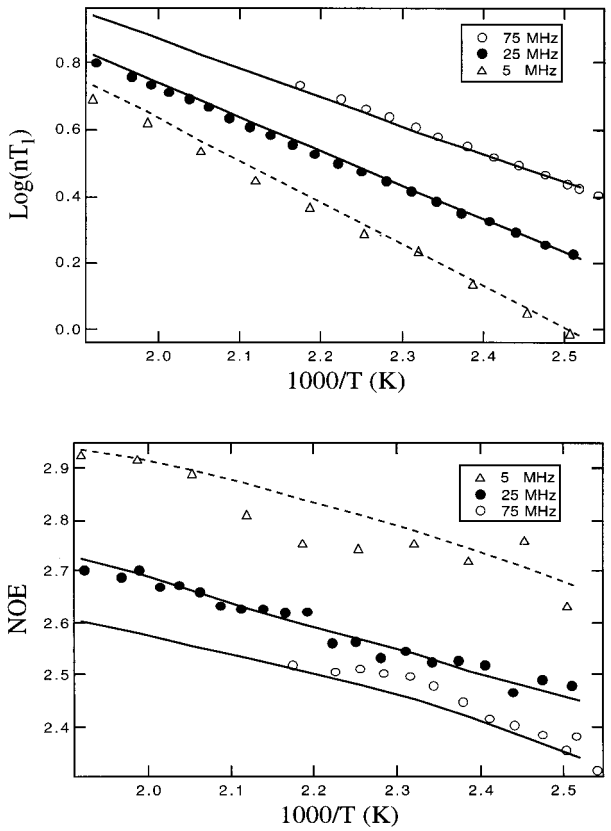

Figure 2. ^{13}C T_1 and NOE of PE2K at 5, 25, and 75 MHz ^{13}C Larmor frequency. Solid lines through the 25 and 75 MHz data are the best fit to the model described in the text. Dashed lines through the 5 MHz data are predictions of this model using the fit parameters for 25 and 75 MHz data. The agreement between the fits, the predictions, and the experimental data shows that the model provides a very good description of the C−H vector reorientation dynamics in PE2K.

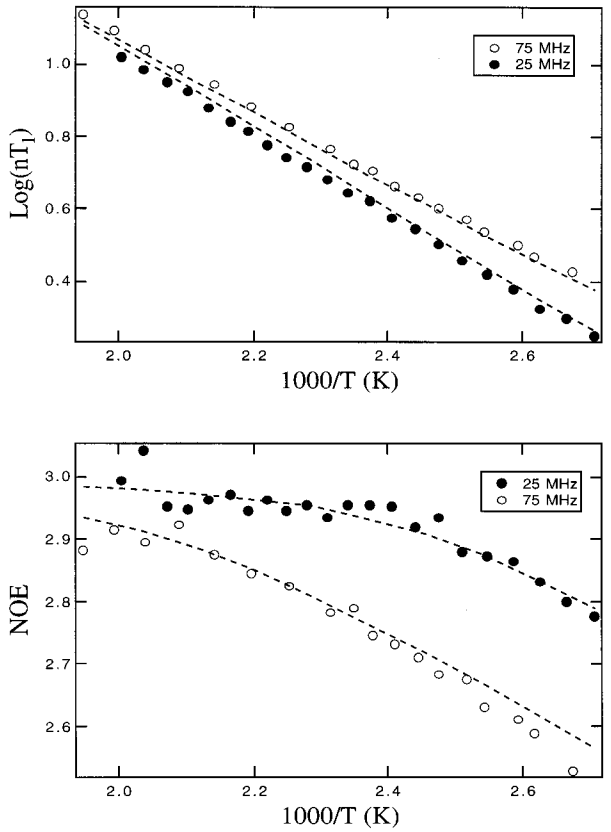

Figure 3. ^{13}C T_1 and NOE of $C_{44}H_{90}$ at 25 and 75 MHz ^{13}C Larmor frequency. Dashed lines through the 25 and 75 MHz data are predictions of the model described in the text. The agreement between the predictions and the experimental data shows that the model provides a reliable way to predict T_1 and NOE values of unentangled polyethylene melts.

frequency even for a very short polyethylene, $C_{44}H_{90}$, as shown in Figure 3. NOE < 3 indicates that the C−H vector OACF has not decayed to zero by a time equal to the inverse of the Larmor frequency. On the same graph, the T_1 value at the highest temperature indicates that conformational dynamics are happening on the picosecond time scale, which is 3 orders of magnitude faster than the inverse of the Larmor frequency. The combination of very fast conformational dynamics and persistent memory of C−H vector orientation shows that there is a significant long time tail in the C−H vector OACF. Therefore, a successful model for fitting the experimental data must incorporate this long time tail.

The model for the C−H vector OACF that best fits the 25 and 75 MHz T_1 and NOE data of PE2K consists of a fast exponential function and a long time tail described by Rouse modes with corrections to higher modes found by MD simulations.

$$G(t) = A_{\text{seg}} \exp\left(-\frac{t}{\tau_{\text{seg}}}\right) + (1 - A_{\text{seg}})G_{\text{Rouse}}(t) \quad (6)$$

$$\tau_{\text{seg}} = \tau_{0,\text{seg}} \exp\left(\frac{E_{\text{a,seg}}}{RT}\right) \quad (7)$$

$$\tau_{\text{R}} = \tau_{0,\text{R}} \exp\left(\frac{E_{\text{a,Rouse}}}{RT}\right) \quad (8)$$

Here $G_{\text{Rouse}}(t)$ is the long time tail part of $G(t)$; $\tau_{0,\text{R}}$ and $E_{\text{a,Rouse}}$ are fitting parameters for the long time tail.

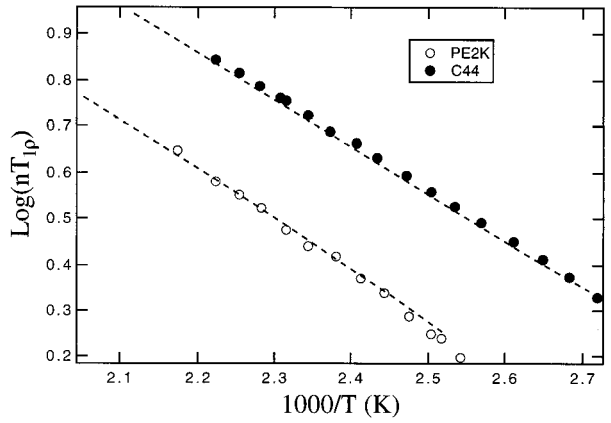

Figure 4. ^{13}C $T_{1\rho}$ at 75 MHz main field and 2 kHz locking field for $C_{44}H_{90}$ and PE2K. Dashed lines through the data are the predictions of the model described in the text. The agreement between the predictions and the experimental data shows that the model is a good description for the global dynamics in these systems.

Since the viscosity of polyethylene melts has an Arrhenius temperature dependence from 150 to 250 °C,[37,38] an Arrhenius temperature dependence is assumed for both the conformational and the global dynamics. All together, there are five fitting parameters in the model: A_{seg}, the temperature-dependent weight of the segmental dynamics;[39] $\tau_{0,\text{seg}}$, the correlation time of the segmental dynamics at infinite temperature; $E_{\text{a,seg}}$, the activation energy of the segmental dynamics; $\tau_{0,\text{R}}$, the longest Rouse time at infinite temperature; and $E_{\text{a,Rouse}}$, the activation energy of the global dynamics.

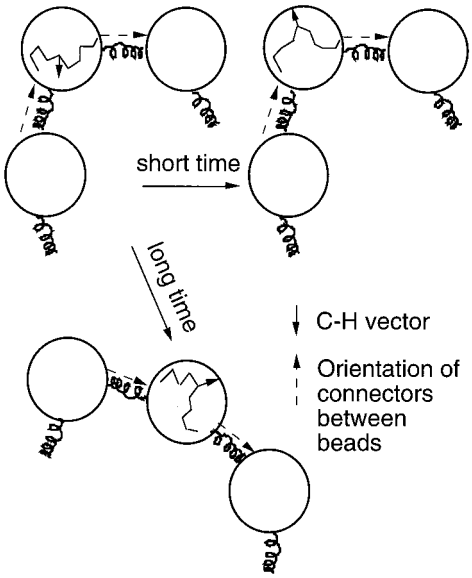

Figure 5. Mapping of C−H vector reorientation in polyethylene onto the bead−spring model. At short times, many conformational transitions take place and partially relax the C−H vector orientation. However, on that short time scale, the vector connecting two beads (the spring vector) cannot reorient significantly, so the C−H vector does not uniformly explore all possible orientations but rather has some tendency to be perpendicular to the spring vector. At long times, which is the time scale of the longest relaxation time of the chain, C−H vector randomization is complete.

Table 1. Contribution of Rouse Modes to M_1 for PE2K

mode	1	2	3	4	5	6	7	8	9	10
$A(a)/A(1)$	1	0.96	0.91	0.86	0.81	0.67	0.58	0.51	0.45	0.41
$\lambda(a)/\lambda(1)$	1	4	9	16	25	42	59	80	105	146

The generation of $G_{\text{Rouse}}(t)$ from Rouse modes is described in ref 40, and an example is given in the Appendix. For a Rouse chain that has n beads and $n-1$ segments of length l_i, one can describe the loss of orientation of the segment $\mathbf{l}_i$ at position i using the time correlation function M_1:

$$M_1^i(t) = \frac{\langle \mathbf{l}_i(t)\, \mathbf{l}_i(0)\rangle}{\langle l_i^2\rangle} \tag{9}$$

After averaging over all or part of the chain, M_1 can be written in terms of Rouse modes:

$$M_1(t) = \sum_{a=1}^{n-1} A(a) \exp\left(-\frac{\lambda_a}{\lambda_1}\frac{t}{\tau_R}\right) \tag{10}$$

$A(a)$ is the amplitude for Rouse mode a, λ_a is the eigenvalue of mode a, and τ_R is the longest Rouse time. MD simulations of $C_{100}H_{202}$[18] found that segments containing 33 carbons or more follow ideal Rouse model predictions. Since PE2K has about 153 carbons, the five longest Rouse modes were taken to be ideal. For higher Rouse modes, the MD simulations found that both the amplitude and the relaxation time deviate from the ideal Rouse model; the simulation results are used for these $A(a)$ and λ_a (see Appendix). A total of 10 modes are needed to give the best fit to the experimental data. The values for $A(a)$ and λ_a of those 10 modes are tabulated in Table 1. From M_1, $G_{\text{Rouse}}(t)$ can be calculated by[40]

Table 2. Values for the Fitting Parameters for PE2K

$\tau_{0,\text{seg}}$ (ps)	$E_{a,\text{seg}}$ (kcal/mol)	A_{seg}[a 39]	$\tau_{0,R}$ (ps)	$E_{a,\text{Rouse}}$ (kcal/mol)
0.034	4.0	$0.915 + 73.957/T - 22688/T^2$	29	5.7

[a] T in kelvin.

$$G_{\text{Rouse}}(t) = 1 - 3\left[x^2 - x^3\left(\frac{\pi}{2}\right)\left[1 - \left(\frac{2}{\pi}\right)\arctan(x)\right]\right] \tag{11}$$

where x is defined as

$$x = \frac{\sqrt{(1 - M_1^2)}}{M_1} \tag{12}$$

$G(t)$ from eq 6 was Fourier transformed to $J(\omega)$, and a global fit was performed to fit T_1 and NOE data at both frequencies.

The results of the best fit to T_1 and NOE experimental data for PE2K at 25 and 75 MHz are plotted as solid lines in Figure 2. Table 2 lists the values of the fitting parameters. Conventional models for fitting NMR relaxation data, such as DLM[7] or log χ^2,[3] do not include a molecular weight-dependent long time tail part and would not fit the data.

We attempted to use various other functions to describe the segmental and the global dynamics of the C−H vector OACF. MD simulations of both $C_{44}H_{90}$[17] and $C_{100}H_{202}$[18] found that the segmental dynamics part of the C−H vector OACF were described by a stretched exponential function with a β value close to 0.5. However, since the conformational dynamics occur at least 100 times faster than the inverse of the Larmor frequencies used in this study, the experimental data are not sensitive to the details of the segmental relaxation; an exponential function and a stretched exponential function generated the same quality fit. These MD simulations found that the long time tail could be well described by a single-exponential function. However, using a single-exponential tail generated a significantly worse fit to our data. Describing the long time tail by a stretched exponential also failed to produce a satisfactory fit to the experimental data. The success of fitting the long time tail to a single exponential in MD simulations[16,18] is probably due to the fact that bad statistics at long times made the simulation less sensitive to the exact shape of the long time tail. Including Rouse modes higher than the 10 longest modes also deteriorated the quality of the fit to our data. These modes correspond to Rouse segments with fewer than 15 carbons, which may significantly deviate from the Gaussian chain approximation. An alternative approach to generate $G_{\text{Rouse}}(t)$ has been proposed by Harnau et al.[41]

B. How Good Is the Model? Figure 2 demonstrates the ability of the model to fit the experimental T_1 and NOE data of PE2K at 25 and 75 MHz. The validity and the accuracy of the model can be further investigated by comparing predictions of the model to experimental studies at other frequencies. The dashed lines through the 5 MHz data of PE2K in Figure 2 are the *predictions* that the model makes using the parameters generated by fitting the 25 and 75 MHz data. Despite some scatter in the experimental NOE at this low frequency, the prediction agrees with the experimental data very well. The same close agreement can be found in Figure 4

Table 3. Comparison between the Fitting Parameter Values for PE2K and the Results from Other Experiments and MD Simulations

	fitting parameter values	results from independent sources	sources
τ_R (ps) at 448 K	17400	13400,[a] 17000[b]	η, D, and $\langle R_G^2 \rangle$ measurements from refs 20−23
$E_{a,Rouse}$ (kcal/mol)	5.7	5.8	η measurements from refs 36, 17
A_{seg} at 450 K	0.967	0.968, 0.970	MD simulations of $C_{44}H_{90}$ from refs 36, 17
τ_{seg} (ps) at 450 K[c]	3.06	2.90, 2.0	MD simulations of $C_{44}H_{90}$ from refs 36, 17
$E_{a,seg}$ (kcal/mol)	4.0	3.1, 3.4	E_a for barrier crossing from refs 42, 29

[a] From ref 31, $\tau_R = 6\eta/NkT\pi^2$. This equation was used with viscosity data[21] for PE with $M_w = 2390$ g/mol at 448 K, correcting for the molecular weight difference by $\tau_R \propto \eta M$. [b] From ref 30, $\tau_R = 2\langle R_g^2 \rangle/\pi^2 D_R$. This equation was used with data[20,22,23] for hydrogenated polybutadiene with $M_w = 2510$ g/mol at 448 K, correcting for molecular weight difference by $\tau_R \propto \eta M$. [c] τ_{seg} is the integral of the part of the correlation function decay due to segmental dynamics.

where the experimental $T_{1\rho}$ of PE2K are plotted against the prediction from the model. The agreement between predictions of the model and independent experimental data supports the validity of the model.

An additional criterion for a good model is that the fitting parameters be consistent with other experiments and MD simulations on similar systems. Table 3 shows a comparison of the fitting parameters with viscosity,[21] self-diffusion coefficient measurements,[20] and MD simulation results.[17,18,29,36,42] The first four fitting parameters agree well with the corresponding experimental and simulation results and further establish the validity of the model. The comparison between $E_{a,seg}$ and the barrier height for conformational transitions is merely suggestive. It is reasonable that the barrier height is a lower bond for $E_{a,seg}$.

C. Predictions for Other Chain Lengths. The success of the model enables a detailed understanding of the dynamics that contribute to C−H vector reorientation in unentangled polyethylene melts. With this knowledge, ^{13}C T_1, NOE, and $T_{1\rho}$ of unentangled polyethylene melts of any molecular weight can be calculated. Since the segmental dynamics involve only a few repeat units,[43] the fitting parameters characterizing the segmental dynamics of PE2K can be used for all polyethylene melts. The longest Rouse time and the activation energy for global dynamics increase/decrease with increasing/decreasing molecular weight. These values can be found or calculated from data in refs 20 and 21.

Figure 3 shows the experimental ^{13}C T_1 and NOE data of $C_{44}H_{90}$ at 25 and 75 MHz ^{13}C Larmor frequency as well as the predictions from the model. Figure 4 shows the experimental ^{13}C $T_{1\rho}$ of $C_{44}H_{90}$ and the prediction from the model. *It should be emphasized here that the dashed lines in Figures 3 and 4 are not fits to the data, but rather predictions using eq 6.* The predictions agree with the experimental data and demonstrate that the model developed is an effective and accurate way to describe the local and global dynamics of unentangled polyethylene melts. The experimental flow activation energy[21] of 4.8 kcal/mol was used as the activation energy of global dynamics for $C_{44}H_{90}$. The longest Rouse time at 448 K was calculated from experimental data,[20,21] resulting in $\tau_{0,R} = 2.98$ ps. Since $C_{44}H_{90}$ is less than one-third as long as PE2K, which contains about 153 carbons, only the three longest Rouse modes were used in the long time tail instead of 10 in the case of PE2K. According to the procedure outlined in section IV.A, corrections were made for Rouse modes with fewer than 33 carbons. Details of the corrections can be found in the Appendix.

D. The Long Time Tail. In contrast to similar studies on other polymers, these experiments on unentangled polyethylene melts are quite sensitive to global dynamics. Figure 6 shows the best fit to the experimental data for PE2K using 10 Rouse modes and using only five Rouse modes. The best fit with five Rouse modes agrees poorly with the experimental data. The fact that including modes 6−10 provides a much better fit indicates that intermediate time scale dynamics between the very fast segmental dynamics and the very slow global dynamics are important for describing the C−H vector reorientation in this system. Fitting the experimental data using the ideal Rouse model for all modes in the long time tail part of the model also generated poor agreement with the experimental data. Therefore, the modifications to the Rouse modes found by the computer simulations[18] are needed for a good fit. This comparison demonstrates the great sensitivity of

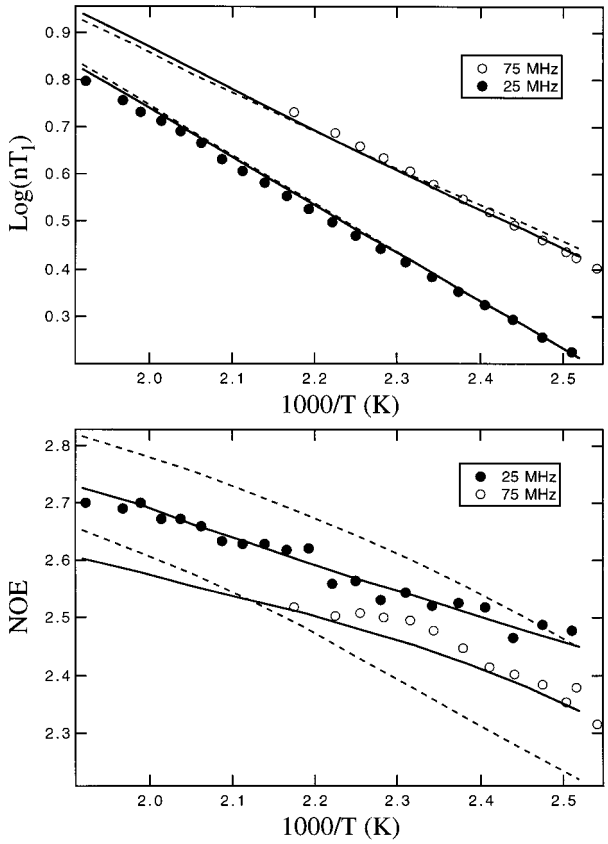

Figure 6. Comparison between modeling the long time tail of PE2K with 10 Rouse modes (solid lines) and modeling with five Rouse modes (dashed lines). The significantly worse fit using five Rouse modes exhibits the great sensitivity of the experimental data toward the global dynamics in the system. It also indicates there are intermediate time scale dynamics between the local conformational dynamics and the longest relaxation time.

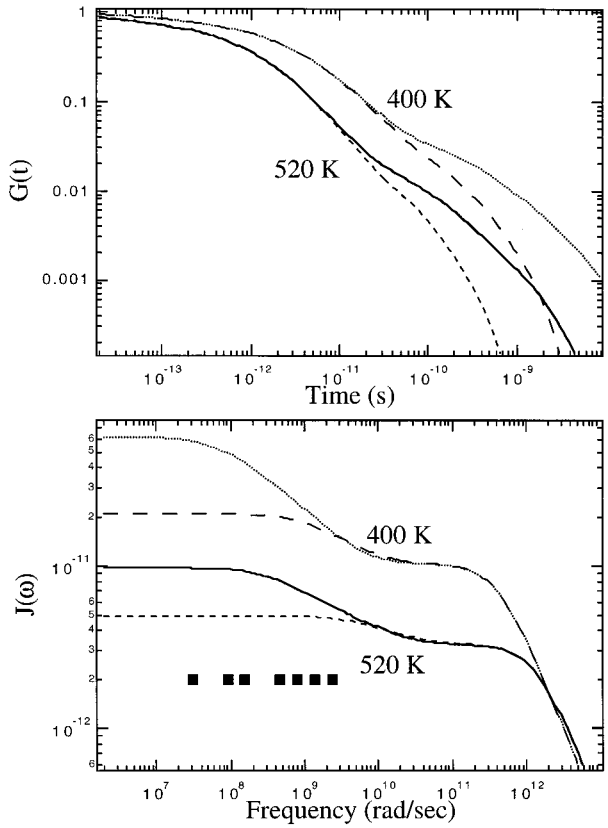

Figure 7. Second-order C−H vector OACF, $G(t)$, described by the model for PE2K and $C_{44}H_{90}$ and the corresponding spectral density functions, $J(\omega)$. The dotted lines are for PE2K at 400 K, the solid lines are for PE2K at 520 K, the long dashed lines are for $C_{44}H_{90}$ at 400 K, and the short dashed lines are for $C_{44}H_{90}$ at 520 K. The frequencies sampled by experiments are represented by squares. The overlap of the long time tails and the experimental frequencies explains why these data are so sensitive to the long time tails in the two systems.

the experimental data to the exact shape of the long time tail.

It is interesting that the global dynamics of polyethylene chains are described accurately in these experiments even though these motions account for only the last 4% of the decay of the C−H vector OACF. The main reason for this is that the time scale for the decay of the long time tail overlaps with the inverse of the Larmor frequencies used. Figure 7 shows the second-order C−H vector OACF, $G(t)$, and its Fourier transform, $J(\omega)$, for the two samples near the two extremes of the temperature covered in this study.[44] The frequencies sampled by the experiment are plotted as filled squares. It is clear from the graph that the frequencies measured by these experiments overlap with the Rouse dynamics over the entire temperature range. The relative insensitivity of these experiments to the details of the local relaxation process mentioned in section IV.A is due to the fact that these relaxations occur at frequencies much higher than the Larmor frequencies in the accessible temperature range.

We speculate that the amplitude of the long time tail in the C−H vector OACF is considerably larger in polyethylene than for many other synthetic polymers. Other polymers studied by T_1 and NOE measurements[7,10,11,45] did not need to account for a long time tail. Computer simulations of polyisoprene,[46] for example, indicate that any long time tail would have an amplitude of less than 2%. Why should the amplitude of this tail be unusually large for polyethylene? We argue below that the lack of side groups in polyethylene allows conformational transitions to occur without the cooperation of the surrounding chains. Thus, conformational transitions take place without significant reorientation of a vector that connects two carbon atoms some distance apart along the chain (perhaps 10−15 atoms). The residual orientation of this vector on the time scale of conformational dynamics determines the amplitude of the long time tail in the C−H vector OACF. Consistent with this hypothesis, we found that atactic polypropylene, with methyl side groups, has a much smaller tail of 0.5%.[47] In a recent ^{1}H double quantum study of polybutadiene,[15] another polymer with no side groups, the authors also noted unexpected strong residual chain order, i.e., a long time tail of unusually large amplitude. This observation is also consistent with our explanation.

E. Are Conformational Transitions the Fundamental Motions for Flow in Polyethylene Melts? The experimental answer to this question requires the comparison of the temperature dependence of conformational dynamics with the temperature dependence of flow. If these two processes have the same temperature dependence, then one imagines that the large-scale rearrangement of chain conformation required for flow is simply the result of many independent conformational transitions. For both $C_{44}H_{90}$ and PE2K, the activation energy for the local dynamics from the fit is 4.0 kcal/mol. A preliminary study on the T_1 and NOE data of a high molecular weight linear polyethylene also shows the same value for the segmental activation energy. On the other hand, the flow activation energy for high molecular weight linear polyethylene is 6.7 kcal/mol.[37,38] The large discrepancy between the two suggests that conformational transitions are not the fundamental motions for flow in polyethylene melts. This result is consistent with earlier dielectric and calorimetric studies[24] of subglass relaxation in polyethylene. Those previous studies found that conformational transitions in polyethylene occur even below T_g and thus could not be the only factor associated with flow at low temperatures. Our new results extend this conclusion to the melt state.

Why is polyethylene different than other polymers in this regard? For polystyrene[48] and atactic polypropylene,[49] for example, it is well established that conformational dynamics have a temperature dependence that is quite similar to that of the viscosity. Again we imagine that the lack of side groups in polyethylene is the critical point. Without side groups, conformational transitions in one chain can occur without requiring transitions in neighboring chains. In the absence of such coupling, conformational transitions are localized to a single chain in a manner similar to the stretching of C−C bonds, and there is no requirement that either of these motions has anything to do with flow.

One possible scenario for this decoupling of flow and conformational dynamics is the following:[50] Since conformational transitions can happen without cooperation from the surrounding chains, they often jump back close to the original conformation without contributing to flow. A small fraction of these conformational transitions happen to coincide with changes in the conformation of neighboring chains, providing a coupled pair of transitions which do contribute to flow. If the fraction of conformational transitions that lead to such coupled

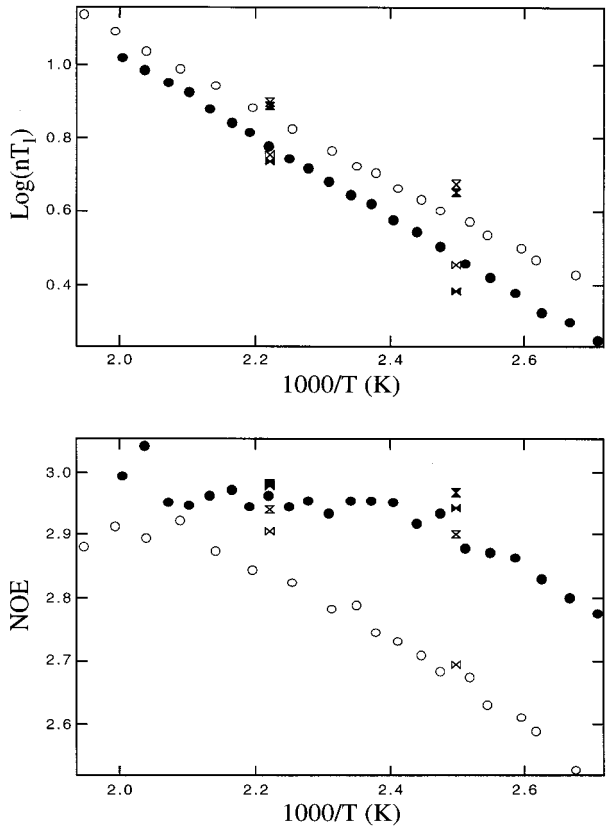

Figure 8. Comparison between NMR experiments and MD simulations[17] for $C_{44}H_{90}$. ^{13}C T_1 and NOE are plotted for 25 MHz (solid circles) and 75 MHz (open circles). Comparison are made with united atom simulations at 25 MHz (filled vertical butterfly) and 75 MHz (open vertical butterfly) and also with explicit atom simulations at 25 MHz (filled horizontal butterfly) and 75 MHz (open horizontal butterfly). The results from explicit atom simulations are in reasonable agreement with the experimental results.

conformational changes is also temperature dependent, the flow activation energy would be higher than the activation energy for conformational dynamics.

F. Comparison with MD Simulations. In developing our model for the C−H vector OACF, we have drawn extensively upon results from molecular dynamics computer simulations.[17,18] The experimental results reported here also can be used to test the quality of these simulations. Since the C−H vector OACF can be calculated from the simulation, and then Fourier transformed to $J(\omega)$, the simulation results can be compared directly to the experimental T_1 and NOE. Figure 8 shows the MD simulation results[17] for $C_{44}H_{90}$ as well as the experimental data. The agreement between the simulation results and the experimental data is the closest yet achieved by any polymer simulations. The united atom model (UA) produced T_1 values higher than the experimental data, and the explicit atom model (EA) produced T_1 values too low. The results are consistent with other comparisons[17,51] showing that UA simulations usually generate faster dynamics than the real system. The UA simulation generated fairly poor agreement with the 25 MHz NOE data, while the EA simulation generated NOE values much closer to the experimental results.

Extensive MD simulations have also been performed on $C_{100}H_{202}$.[18] Although we have not acquired experimental data on this material, we can still make an interesting comparison with our results. Since our experimental results on PE2K (about 153 carbons per chain) and the use of our model allowed a quantitative prediction of the results for $C_{44}H_{90}$, we expect that we can also predict the experimental results for $C_{100}H_{202}$ with similar accuracy (roughly 10%). In Table 4 we show the results of this prediction for 90 MHz ^{13}C Larmor frequency. These predicted values are compared to simulation results reported in ref 18. The results from the simulation are in reasonable agreement with our predictions but indicate that the local relaxation times in the simulation are 20−30% too slow.

Table 4. Comparison of Predicted T_1 and NOE vs MD Simulation Results of $C_{100}H_{202}$ at 509 K

	nT_1 (s)	NOE
predicted	9.1	2.65
MD simulation (UA)	7.2	2.38
MD simulation (EA)	6.0	2.75

G. Comparison with Other Models. Brereton et al. have developed an elegant theory[13] for describing the contribution of global dynamics to NMR relaxation of entangled and unentangled polymer melts. This model has been applied to both proton[52] and deuterium[53] NMR measurements. It is appropriate to comment briefly upon this approach since it would be an alternate method of interpreting our experimental results. While this model has considerable potential for a general description of NMR relaxation in polymer melts, the current implementation of the model has some problems that do not allow a quantitative description of our experiments. One problem is that T_2 is sensitive to high-frequency components in the spectral density which are not accounted for in the analysis of refs 52 and 53. For our ^{13}C data on unentangled polyethylene melts, these high-frequency components are the major influence on T_2 so their neglect is serious (in this regime, $T_2 = T_{1\rho}$). At least partially as a result of this, the model does not provide quantitative information about relaxation times. From proton experiments on unentangled polyethylene melts, the theory was used to extract parameters that characterize the Rouse modes.[52] From these fit parameters, one can calculate that the longest relaxation time for a chain with $M_w = 2150$ g/mol is predicted to be 440 ns at 422 K. Comparison with the experimental values in Table 3 indicates that these predictions are about 20 times too long. (The temperature difference between 448 and 422 K only changes the longest relaxation time by a factor of 1.5.)

V. Conclusion

^{13}C T_1, NOE, and $T_{1\rho}$ at 5, 25, and 75 MHz ^{13}C Larmor frequency were measured for two unentangled polyethylene melts. A model that incorporates fast segmental relaxation and a long time tail described by Rouse modes was found to be able to fit all the experimental data. The fitting parameters are consistent with independent experimental results such as viscosity and self-diffusion coefficients and also with MD simulations. Using the model, one can predict T_1 and NOE values of unentangled polyethylene of any molecular weight. The activation energy for the conformational dynamics was determined to be 4.0 kcal/mol, significantly less than the flow activation energy for polyethylene melts. Therefore, conformational transitions are not the fundamental motions for flow for polyethylene. Comparison with MD simulations showed that an explicit atom model reproduced the experimental data reasonably well.

Our next step is to collect experimental data and develop a similar model for C−H vector reorientation in entangled polyethylene melts. The success of this project would not only characterize the global dynamics in the much less understood crossover and entangled region but also enable us to predict T_1, NOE, and $T_{1\rho}$ values of high molecular weight polyethylene melts. Such information could be used to aid in the characterization of long branches in polyethylene melts, a very important industrial problem.[54,55] Alternative models for characterizing the long time tail including the Brereton model will be reexamined with the entangled PE work.

Acknowledgment. This research is supported by the National Science Foundation through the Division of Material Research, Polymer Program (DMR-9732483). Most of the study was performed on a variable field NMR supported by NSF CHE 95-08244. Part of the preliminary study was performed in the Instrument Center of the Department of Chemistry, University of Wisconsin—Madison. Those instruments are supported by NSF CHE-8306121 and NIH 1 S10 RR02388-01. We thank Prof. Tom Farrar, Marvin Kontney, and Tom Ferris for their support. We also thank Prof. Marina Guenza and Prof. Angelo Perico for teaching us how to calculate $G(t)$ from the ideal Rouse model.

Appendix

The following procedure was used to calculate the spectral density function from Rouse modes as described in the text. Details are given here for the example of polyethylene with $M_w = 2150$ g/mol. All the equations used here are from Perico and Guenza.[40]

An infinite Rouse chain approximation (N normal modes, $N \rightarrow \infty$) is used, and corrections are made to only include the center 80% of the chain. The 10% at each end should be excluded because the end six carbons have different chemical shifts. Carbons near the end that have a similar chemical shift have slightly different T_1's depending on their positions on the chain; those near the end have the longest T_1's, and those at the center have the shortest T_1's. Since the way the experiment was conducted favored the short T_1's, some systematic bias was introduced. Calculations indicate that discounting 10% of the carbons closest to the ends introduces the same bias as introduced by the experimental procedures. Therefore, only the center 80% of the chain is used.

For a Rouse chain that has n beads and $n - 1$ segments, the time autocorrelation function M_1 (defined by eq 9) is used to describe how the orientation of the segment i is lost due to Brownian motion.

$$M_1^i(t) = \sum_{a=1}^{n-1} (\Delta_a^i)^2 \mu_a^{-1} \exp\left(-\frac{\lambda_a}{\lambda_1}\frac{t}{\tau_R}\right) \tag{A1}$$

where

$$\Delta_a^i = Q_{ia} - Q_{i-1,a} \tag{A2}$$

For the melt, hydrodynamic interactions are negligible and $\mu_a = \lambda_a$. Equations for Q and λ are[30]

$$\lambda_a = 4 \sin^2\left(\frac{\pi a}{2n}\right) \tag{A3}$$

$$Q_{ia} = \sqrt{\frac{2}{n}}\left[\cos\frac{\pi a(i - 0.5)}{n}\right] \quad \text{for } 0 < a < n,\ 0 < i < n \tag{A4}$$

where a is the mode number and n is the number of beads in the Rouse chain. i is the segment number which runs from 1 to $n - 1$. Note that a chain with n beads has n modes, but they are numbered from 0 to $n - 1$, and the zero mode is center-of-mass translation (thus not included in our sum).

Since only the center 80% of the segments are needed, eq A1 can be written as

$$M_1(t) = \frac{1}{0.8N}\sum_{i=0.1N}^{0.9N} M_1^i(t) = \sum_{a=1}^{n-1} \exp\left(-\frac{\lambda_a}{\lambda_1}\frac{t}{\tau_R}\right)\left\{\left[\frac{1}{0.8N}\sum_{i=0.1N}^{0.9N}(\Delta_a^i)^2\right]\frac{1}{\lambda_a}\right\} \tag{A5}$$

The second equality comes from reordering the summations. Note that the quantity in the curly brackets is just an amplitude factor for each Rouse mode, designated as $A(a)$:

$$A(a) = \left[\frac{1}{0.8N}\sum_{i=0.1N}^{0.9N}(\Delta_a^i)^2\right]\frac{1}{\lambda_a} \tag{A6}$$

Then M_1 can be written as

$$M_1(t) = \sum_{a=1}^{n-1} A(a) \exp\left(-\frac{\lambda_a}{\lambda_1}\frac{t}{\tau_R}\right) \tag{A7}$$

In the MD simulation of $C_{100}H_{202}$,[18] only the three longest Rouse modes follow ideal Rouse dynamics, which means beads with more than 33 carbons follow ideal Rouse model. For PE2K, the same criterion means the five longest Rouse modes follow ideal Rouse model. Therefore, $A(a)$ and λ_a for the first five modes are directly imported from eqs A6 and A3. Their values are normalized to the longest mode λ_1 and $A(1)$ by $\lambda_i' = \lambda_i/\lambda_1$ and $A'(i) = A(i)/A(1)$:

$$\lambda_1' = 1;\ \lambda_2' = 4;\ \lambda_3' = 9;\ \lambda_4' = 16;\ \lambda_5' = 25$$

$$A'(1) = 1;\ A'(2) = 0.96;\ A'(3) = 0.91;\ A'(4) = 0.86;\ A'(5) = 0.81$$

For the higher modes, the results from the simulation are used to determine the value of $A(a)$ and λ_a. The simulation found a $1/p^3$ dependence for the mean-square mode amplitude. The ideal Rouse model predicts a $1/p^2$ dependence. For $A(a)$, the ideal Rouse model predicts no p dependence; therefore, $1/p$ dependence is used for higher modes according to the findings of the simulations. The simulation also found that the relaxation times for the higher modes deviate from the $1/p^2$ prediction of the ideal Rouse model. Therefore, integration of the curves (Figure 11 in ref 18) for the autocorrelation function of each mode in the simulation paper was conducted, and the relaxation time for those higher modes was estimated:

$$\lambda_6' = 42;\ \lambda_7' = 59;\ \lambda_8' = 80;\ \lambda_9' = 105;\ \lambda_{10}' = 146$$

$$A'(6) = 0.67;\ A'(7) = 0.58;\ A'(8) = 0.51;\ A'(9) = 0.45;\ A'(10) = 0.41$$

The $A(a)$'s and λ_a's are inserted into eq A7. The C−H vector OACF and $G_{\text{Rouse}}(t)$ can then be calculated using eqs 11 and 12.[40] Equations 11 and 12 are exact for the Rouse model but only approximate for real chains which deviate from Gaussian statistics. Previous work has shown that these equations are a reasonable approximation even for systems that are strongly non-Gaussian.[56] Thus, for the present application where only small deviations from Gaussian behavior are likely, we expect these equations to be an excellent approximation.

The resulting $G_{\text{Rouse}}(t)$ function cannot be Fourier transformed analytically so an approximation of the function is made with a sum of exponentials. Seven exponentials are enough to approximate the function from time zero up to 10 times the longest Rouse time. Those seven exponentials are then inserted as $G_{\text{Rouse}}(t)$ in eq 6, and the resulting $G(t)$ is Fourier transformed analytically to yield the spectral density function from which T_1 and NOE values can be calculated. A grid search strategy is employed to adjust the fitting parameters to produce the best fit to the 25 and 75 MHz ^{13}C Larmor frequency T_1 and NOE data of PE2K.

In the case of $C_{44}H_{90}$, only the longest Rouse mode has more than 33 carbons so the ideal Rouse model scaling is not used. Since only 10 modes are used for PE2K, only three longest modes are employed in this system. Discounting the 10 carbons at each end gives further correction to $A(a)$ as can be calculated by eq A6. Following the same procedure described above, λ_a and $A(a)$ are calculated as

$$\lambda_1' = 1;\ \lambda_2' = 4.7;\ \lambda_3' = 10.8$$

$$A'(1) = 1;\ A'(2) = 0.38;\ A'(3) = 0.20$$

References and Notes

(1) McCall, D. W. *Acc. Chem. Res.* **1971**, *4*, 223.
(2) Moe, N. E.; Ediger, M. D. *Macromolecules* **1996**, *29*, 5484.
(3) Schaefer, J. *Macromolecules* **1973**, *6*, 882.
(4) Jones, A. A.; Stockmayer, W. H. *J. Polym. Sci., Polym. Phys. Ed.* **1977**, *15*, 847.
(5) Bendler, J. T.; Yaris, R. *Macromolecules* **1978**, *11*, 1650.
(6) Helfand, E. *J. Chem. Phys.* **1971**, *54*, 4651.
(7) Dejean de la Batie, R.; Lauprêtre, F.; Monnerie, L. *Macromolecules* **1988**, *21*, 2045.
(8) Hall, C. K.; Halfand, E. *J. Chem. Phys.* **1982**, *77*, 3275.
(9) Lipari, G.; Szabo, A. *J. Am. Chem. Soc.* **1982**, *104*, 4546.
(10) Baysal, C.; Erman, B.; Bahar, I.; Lauprêtre, F.; Monnerie, L. *Macromolecules* **1997**, *30*, 2058.
(11) Dejean de la Batie, R.; Lauprêtre, F.; Monnerie, L. *Macromolecules* **1988**, *21*, 2052.
(12) Cohen-Addad, J. P.; Dupeyre, R. *Polymer* **1983**, *24*, 400.
(13) Brereton, M. G. *J. Chem. Phys.* **1991**, *94*, 2136.
(14) Kimmich, R.; Köpf, M.; Callaghan, P. *J. Polym. Sci., Polym. Phys. Ed.* **1991**, *29*, 1025.
(15) Graf, R.; Heuer, A.; Spiess, H. W. *Phys. Rev. Lett.* **1998**, *80*, 5738.
(16) Smith, G. D.; Yoon, D. Y.; Zhu, W.; Ediger, M. D. *Macromolecules* **1994**, *27*, 5563.
(17) Paul, W.; Yoon, D. Y.; Smith, G. D. *J. Chem. Phys.* **1995**, *103*, 1702.
(18) Paul, W.; Smith, G. D.; Yoon, D. Y. *Macromolecules* **1997**, *30*, 7772.
(19) McKenna, G. B.; Ngai, K. L.; Plazek, D. J. *Polymer* **1985**, *26*, 1651.
(20) Pearson, D. S.; Fetters, L. J.; Graessley, W. W.; Ver Strate, G.; von Meerwall, E. *Macromolecules* **1994**, *27*, 711.
(21) Pearson, D. S.; Ver Strate, G.; von Meerwall, E.; Schilling, F. C. *Macromolecules* **1987**, *20*, 1133.
(22) Horton, J. C.; Squires, G. L.; Boothroyd, A. T.; Fetter, L. J.; Rennie, A. R.; Glinka, C. J.; Robinson, R. A. *Macromolecules* **1989**, *22*, 681.
(23) Boothroyd, A. T.; Rennie, A. R.; Boothroyd, C. B. *Europhys. Lett.* **1991**, *15*, 715.
(24) Boyd, R. H. *Polymer* **1985**, *26*, 323.
(25) Harmandaris, V. A.; Mavrantzas, V. G.; Theodorou, D. N. *Macromolecules* **1998**, *31*, 7943.
(26) Paul, W.; Smith, G. D.; Yoon, D. Y.; Farago, B.; Rathgeber, S.; Zirkel, A.; Willner, L.; Richter, D. *Phys. Rev. Lett.* **1998**, *80*, 2346.
(27) Kostov, K. S.; Freed, K. F.; Webb III, E. B.; Mondello, M.; Grest, G. S. *J. Chem. Phys.* **1998**, *108*, 9155.
(28) Jin, Y.; Boyd, R. H. *J. Chem. Phys.* **1998**, *108*, 9912.
(29) Boyd, R. H.; Gee, R. H.; Han, J.; Jin, Y. J. *J. Chem. Phys.* **1994**, *101*, 788.
(30) Doi, M.; Edwards, S. F. *The Theory of Polymer Dynamics*; Claredon: Oxford, 1986.
(31) Aklonis, J. J.; MacKnight, W. J. *Introduction to Polymer Viscoelasticity*; Wiley: New York, 1983.
(32) Qiu, X., to be published.
(33) Glowinkowski, S.; Gisser, D. J.; Ediger, M. D. *Macromolecules* **1990**, *23*, 3520.
(34) Ohuchi, M.; Fujito, T.; Imanari, M. *J. Magn. Reson.* **1979**, *35*, 415.
(35) Heatley, F. *Annu. Rep. NMR Sepctrosc.* **1986**, *17*, 179 and reference therein.
(36) Smith, G. D.; Yoon, D. Y.; Jaffe, R. L. *Macromolecules* **1995**, *28*, 5897.
(37) Mendelson, R. A.; Bowles, W. A.; Finger, G. L. *J. Polym. Sci., Part A-2* **1970**, *8*, 105.
(38) Raju, V. R.; Smith, G. G.; Marin, G.; Knox, J. R.; Graessley, W. W. *J. Polym. Sci., Polym. Phys. Ed.* **1979**, *17*, 1183.
(39) Although the exact mechanism for the temperature dependence of A_{seg} is unresolved, fitting the experimental data with a temperature-independent A_{seg} resulted in very poor quality fit. Therefore, A_{seg} was allowed to freely change with temperature. The resulting values are described by the empirical function given in Table 2.
(40) Perico, A.; Guenza, M. *J. Chem. Phys.* **1985**, *83*, 3103.
(41) Harnau, L.; Winkler, R. G.; Reineker, P. *Europhys. Lett.* **1999**, *45*, 488.
(42) Smith, G. D.; Yoon, D. Y. *J. Chem. Phys.* **1994**, *100*, 649.
(43) Moe, N. E.; Ediger, M. D. *Macromolecules* **1995**, *28*, 2329.
(44) In Figure 8, the fast segmental relaxation was represented as a stretched exponential with $\beta = 0.5$ that has the same correlation time as the single exponential used in the model. Both representations are consistent with the experimental results. On the basis of MD simulations, we expect that the stretched exponential form is more realistic.
(45) Moe, N. E.; Qiu, X.; Ediger, M. D., submitted to *Marcomolecules*.
(46) Moe, N. E.; Ediger, M. D. *Polymer* **1996**, *37*, 1787.
(47) Qiu, X.; Ediger, M. D., to be submitted to *J. Chem. Phys.*
(48) Schaefer, D.; Spiess, H. W.; Suter, U. W.; Fleming, W. W. *Macromolecules* **1990**, *23*, 3431.
(49) Zemke, K.; Schmidt-Rohr, K.; Spiess, H. W. *Acta Polym.* **1994**, *45*, 148.
(50) Ideas stimulated from private communications with Dr. Wolfgang Paul.
(51) Smith, G. D.; Paul, W.; Richter, D.; Qiu, X.; Ediger, M. D., to be submitted.
(52) Brereton, M. G.; Ward, I. M.; Boden, N.; Wright, P. *Macromolecules* **1991**, *24*, 2068.
(53) Klein, P. G.; Adams, C. H.; Brereton, M. G.; Ries, M. E.; Nicholson, T. M.; Hutchings, L. R.; Richards, R. W. *Macromolecules* **1998**, *31*, 8871.
(54) Hansen, E. W.; Blom, R.; Bade, O. M. *Polymer* **1997**, *38*, 4295.
(55) ben Cheick Larbi, F.; Hert, M.; Grenier, M.; Rault, J. *Macromolecules* **1985**, *18*, 164.
(56) See Figure 5 of: Perico, A.; Moe, N. E.; Ediger, M. D. *J. Chem. Phys.* **1998**, *108*, 1245.

MA991086N